Ultrafast saturation of electronic-resonance-enhanced coherent anti-Stokes Raman scattering and comparison for pulse durations in the nanosecond to femtosecond regime

Anil K. Patnaik,[1,2,*] Sukesh Roy,[3,†] and James R. Gord[1,‡]

[1]*Air Force Research Laboratory, Aerospace Systems Directorate, Wright-Patterson Air Force Base, Ohio 45433, USA*
[2]*Department of Physics, Wright State University, Dayton, Ohio 45435, USA*
[3]*Spectral Energies, LLC, 5100 Springfield Street, Dayton, Ohio 45431, USA*

The saturation threshold of a probe pulse in an ultrafast electronic-resonance-enhanced (ERE) coherent anti-Stokes Raman spectroscopy (CARS) configuration is calculated. We demonstrate that while the underdamping condition is a sufficient condition for saturation of ERE-CARS with the long-pulse excitations, a transient gain must be achieved to saturate the ERE-CARS signal for the ultrafast probe regime. We identify that the area under the probe pulse can be used as a definitive parameter to determine the criterion for a saturation threshold for ultrafast ERE-CARS. From a simplified analytical solution and a detailed numerical calculation based on density-matrix equations, the saturation threshold of ERE-CARS is compared for a wide range of probe-pulse durations from the 10-ns to the 10-fs regime. The theory explains both qualitatively and quantitatively the saturation thresholds of resonant transitions and also gives a predictive capability for other pulse duration regimes. The presented criterion for the saturation threshold will be useful in establishing the design parameters for ultrafast ERE-CARS.

I. INTRODUCTION

Femtosecond-laser-based coherent anti-Stokes Raman spectroscopy (CARS) has been used extensively in time-resolved nonlinear spectroscopy research in recent years [1]. A variant of CARS, a doubly resonant four-wave-mixing scheme, where a probe pulse *resonant* to the electronic transition scatters off the Raman coherence generated by the Raman-resonant pump and Stokes pulses, is known as electronic-resonance-enhanced CARS (ERE-CARS) [2]. This technique is capable of obtaining a few orders of magnitude enhancement of the CARS signal as compared to traditional CARS with a nonresonant probe [3–5]. Also, since the ERE-CARS technique is inherently quenching independent [6,7], this technique has been employed very successfully using nanosecond lasers for measuring the concentration of minor species such as NO [2,6,8–12], which is a tracer pollutant in combustion processes [13]. However, since the resonant probe in the ERE-CARS configuration interacts strongly with the molecules, the saturation limit of the probe intensity is lower than that in conventional CARS [14]. It has been observed that to maximize the signal-to-noise ratio (SNR), the nanosecond ERE-CARS setup operates near the saturation limit of the probe intensity [15]. In such spectroscopic techniques, while it is important to obtain the spectrum of the intended molecule in the generated ERE-CARS signal with an acceptable SNR, saturation can alter the spectral signature (such as the Stark shift of transitions [16]), requiring additional model corrections such as those employed in saturation of fluorescence [17], four-wave mixing [18,19], and standard off-resonance CARS [20]. With the ultrafast-laser excitations, since the operating intensities of the lasers are generally much higher than those used in nanosecond ERE-CARS experiments

and the duration of exciting pulses is much shorter than the molecular decay and dephasing time scales, it is very important to understand the ultrafast saturation dynamics of the ERE-CARS.

Recently, we demonstrated that the physics of ultrafast saturation of elementary optical processes (such as absorption and fluorescence) differs significantly for different durations of the pumping laser pulses [21,22]. It was shown that in an underdamping regime, i.e., if the Rabi frequency associated with a long-pulse or cw laser is greater than the effective decay rate of the system, absorption and fluorescence saturation can occur [23,24]. However, for short pulses when the pulse duration of the pump is shorter than the effective decoherence time scales of molecule, the saturation of ultrafast absorption occurs only when the pulse drives the molecule to a transient-gain regime. Such differences in the saturation of polarization spectroscopy with long and short pulses have been reported earlier [25,26]. The ultrafast saturation limit could be predicted quantitatively by employing the pulse area [27] as the deterministic parameter, and the same argument is extended to saturation of the Raman transition [22]. Note that the saturation threshold of the probe-pulse intensity in a traditional CARS is much higher than the ERE-CARS setup because of far weaker off-resonance interaction of the probe with the molecular transition [21]. Although saturation of ERE-CARS with long-pulse excitation has been extensively studied [7,14], the saturation of the ultrafast ERE-CARS is never discussed.

In this paper, we generalize study of ultrafast saturation of emission for quantitative determination of the threshold of saturation of ultrafast ERE-CARS. Saturation of the ultrafast-CARS signal with an off-resonance probe setup was discussed in Ref. [21]. Here we obtain a quantitative saturation criterion for the probe intensity to determine the threshold of saturation of ultrafast ERE-CARS using the area under the probe pulse. We compare the calculated threshold of saturation for a range of short- and long-pulse-duration probe pulses to compare and fundamentally distinguish the saturation processes for those

---

*anil.patnaik@wright.edu
†roy.sukesh@gmail.com
‡james.gord@us.af.mil

durations. We show that the pulse-area-based criterion for saturation of ERE-CARS is valid for shorter pulses and is accurate for the delayed probe conditions. Our study is valid for ultrashort pulses where the rotating-wave approximation is still valid, i.e., the Rabi frequency is much smaller than the optical frequency [28]. Also, the propagation effect is not considered. Note that the ultrafast saturation reported here is on a time scale of the vibrational period of molecules [29] and is orders of magnitude faster than state-of-the-art electronic switches. This study provides predictive capability for the intensity threshold to avoid ERE-CARS saturation, which is very important for establishing design parameters needed for ultrafast spectroscopic measurements. Other interesting applications may include saturation-based femtosecond switches and controllable wave-packet dynamics [30], above-saturation-threshold spectroscopy [31], and enhanced spatial and spectral resolution via saturated CARS [32].

The paper is organized as follows. In Sec II we discuss the model and derive a density matrix equation to calculate ERE-CARS polarization. In Sec. III we obtain approximate analytical and numerical solutions to understand the ultrafast dynamics of the molecule under the influence of the strong probe laser. The ultrafast saturation of the signal in a hybrid ERE-CARS configuration is presented and the effect of probe delay on saturation is discussed in Sec. IV. A comparison of the saturation criterion is obtained numerically and compared with analytical results for a wide range of probe-pulse durations in Sec. V. The results are summarized in Sec. VI.

II. MODEL CALCULATION FOR ERE-CARS POLARIZATION

We consider a six-level system for studying the saturation of ERE-CARS from nanosecond to femtosecond excitation regimes, as depicted in Fig. 1. The system parameters used for the calculation are kept close to those of an NO molecule. The
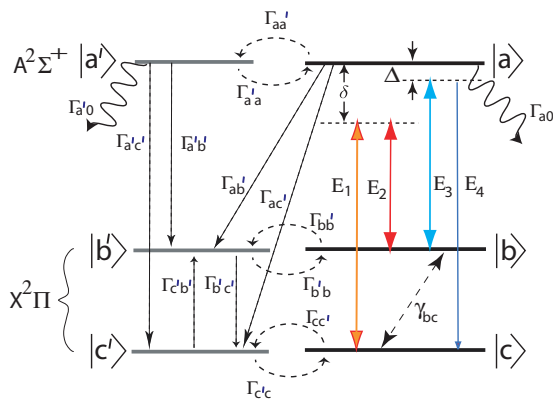

FIG. 1. Six-level model used for studying ERE-CARS saturation of NO. The rotational manifolds in the ground (excited) vibrational state in the ground electronic state $X\,^2\Pi$ are represented by $|c\rangle$ and $|c'\rangle$ and rovibrational states in the excited electronic state $A\,^2\Sigma^+$ are represented by $|a\rangle$ and $|a'\rangle$. The pump, Stokes, probe, and generated CARS pulses that are represented by E_1, E_2, E_3, and E_4, respectively, couple the unprimed states $|a\rangle$, $|b\rangle$, and $|c\rangle$. The prime states are considered to be the bath levels to account for all of the decays Γ_{ij} in the system and the coherence dephasing is represented by γ_{ij}.

energy levels $|a\rangle$ and $|a'\rangle$ could correspond to a rovibrational state in the excited electronic state $A\,^2\Sigma^+(v=0)$. The energy levels $|b\rangle$ and $|b'\rangle$ ($|c\rangle$ and $|c'\rangle$) are the rovibrational states in the $v=1$ ($v=0$) vibrational manifolds in the ground electronic state $X\,^2\Pi$. The primed states are representative states of the rotational manifold within the same vibrational states as the corresponding unprimed states and they are used as bath levels for accurately taking into account the various decays such as rotational-energy transfer (RET), vibrational-energy transfer, electronic decay, and quenching rates of the NO molecule. The population-decay and coherence-dephasing time scales vary in the nanosecond to picosecond range; hence, the corresponding rates are important in attaining accurate ERE-CARS results in the nanosecond- and picosecond-excitation regimes. However, the decays and dephasing rates play very insignificant roles in time-resolved signal detection in the femtosecond-excitation regime. For a detailed discussion about the decays and dephasing parameters used in the modeling of the NO molecule, see Ref. [7]. Furthermore, note that a short pulse may couple multiple rotational states in each vibrational manifold simultaneously because of the broad bandwidth associated with the pulse that affects the saturation dynamics of the CARS signal [21]. However, since the goal of this work is to obtain an analytical understanding of the saturation threshold of ERE-CARS for pulse durations ranging from nanoseconds to femtoseconds, we limit our model to pump-, Stokes-, and probe-pulse coupling to only three of the molecular levels.

Three input pulses $\vec{E}_i$ ($i \to 1,2,3$) at frequencies ν_i generate the CARS signal $\vec{E}_4$ at a frequency $\nu_4 = \nu_1 - \nu_2 + \nu_3$. The pump ($\vec{E}_1$) and Stokes ($\vec{E}_2$) pulses are in two-photon resonance with the Raman transition $|b\rangle \leftrightarrow |c\rangle$ to generate the Raman coherence ρ_{bc}. The probe $\vec{E}_3$ couples to the electronic transition via $|a\rangle \leftrightarrow |b\rangle$ resonantly or near resonantly with a detuning of Δ. All of the input pulses are given by

$$\vec{E}_i(t) = \hat{e}_i E_i(t) e^{-i\nu_i t} + \text{c.c.}, \qquad (1)$$

with Gaussian envelope functions

$$E_i(t) = E_{i0} e^{-(t-t_i)^2/\tau_i^2}. \qquad (2)$$

Here E_{i0}, $\hat{e}_i$, t_i, and τ_i are the peak electric field, polarization, peak position of the pulse, and duration of the pulse of the applied fields, respectively ($i \to 1,2,3$). All of the fields are assumed to be linearly polarized and are parallel to each other and parallel to the induced dipole moments corresponding to their respective transitions. The total Hamiltonian is given by

$$\mathcal{H} = \hbar(\omega_{ac} A_{aa} + \omega_{bc} A_{bb} + \omega_{a'c} A_{a'a'} + \omega_{b'c} A_{b'b'})$$
$$- \hbar[\Omega_1 e^{-i\nu_1 t} A_{ac} + (\Omega_2 e^{-i\nu_2 t} + \Omega_3 e^{-i\nu_3 t})A_{ab} + \text{H.c.}],$$
$$(3)$$

where $\hbar\omega_{\alpha c}$ is the energy separation between the states α and the ground state c ($\alpha \to a,b,a',b'$). The projection operators $A_{\alpha\beta} = |\alpha\rangle\langle\beta|$ correspond to the population (coherence) for $\alpha = \beta$ ($\alpha \neq \beta$), where $\alpha,\beta \to a,b,c,a',b',c'$. Note that the primed states are assumed to be degenerate with the corresponding unprimed states for simplicity. The Rabi frequencies corresponding to the incident fields are

denoted by

$$\Omega_1 = \vec{d}_{ac} \cdot \hat{e}_1 E_1(t)/\hbar,$$
$$\Omega_2 = \vec{d}_{ab} \cdot \hat{e}_2 E_2(t)/\hbar, \qquad (4)$$
$$\Omega_3 = \vec{d}_{ab} \cdot \hat{e}_3 E_3(t)/\hbar.$$

Here $\vec{d}_{ab}$ ($\vec{d}_{ac}$) is the transition matrix element that includes the induced dipole moment, Frank-Condon factors, and the rotational-overlapping function between the rovibrational levels $|a\rangle \rightarrow |b\rangle$ ($|a\rangle \rightarrow |c\rangle$).

The Liouville equation to describe the dynamics of the molecule-laser interaction for the model system can be obtained as

$$\frac{\partial \rho}{\partial t} = -\frac{i}{\hbar}[\mathcal{H}, \rho(t)] + \mathcal{L}\rho(t), \qquad (5)$$

where $\mathcal{L}$ is the Liouville operator consisting of the phenomenological decay (dephasing) rates of the molecular-state population (coherences). Substituting Eq. (3) into Eq. (5) and writing explicitly all of the phenomenological decay and dephasing rates of the system, the equations for the density-matrix elements can be written as

$$\dot{\rho}_{aa} = -\Gamma_a \rho_{aa} + \Gamma_{a'a} \rho_{a'a'} + [i\Omega_1 e^{-i\nu_1 t} \rho_{ca}$$
$$+ i(\Omega_2 e^{-i\nu_2 t} + \Omega_3 e^{-i\nu_3 t})\rho_{ba} + \text{c.c.}],$$
$$\dot{\rho}_{ab} = -(\gamma_{ab} + i\omega_{ab})\rho_{ab} + i\Omega_1 e^{-i\nu_1 t} \rho_{bc}^*$$
$$+ i(\Omega_2 e^{-i\nu_2 t} + \Omega_3 e^{-i\nu_3 t})(\rho_{bb} - \rho_{aa}),$$
$$\dot{\rho}_{ac} = -(\gamma_{ac} + i\omega_{ac})\rho_{ac} + i(\Omega_2 e^{-i\nu_2 t} + \Omega_3 e^{-i\nu_3 t})\rho_{bc}$$
$$+ i\Omega_1 e^{-i\nu_1 t}(\rho_{cc} - \rho_{aa}),$$
$$\dot{\rho}_{bb} = -\Gamma_{bb'}\rho_{bb} + \Gamma_{b'b}\rho_{b'b'}$$
$$- [i(\Omega_2 e^{-i\nu_2 t} + \Omega_3 e^{-i\nu_3 t})\rho_{ab} + \text{c.c.}], \qquad (6)$$
$$\dot{\rho}_{bc} = -(\gamma_{bc} - i\omega_{bc})\rho_{bc} + i(\Omega_2^* e^{i\nu_2 t} + \Omega_3^* e^{i\nu_3 t})\rho_{ac}$$
$$- i\Omega_1 e^{-i\nu_1 t} \rho_{ba},$$
$$\dot{\rho}_{cc} = -\Gamma_{cc'}\rho_{cc} + \Gamma_{c'c}\rho_{c'c'} - [i\Omega_1 e^{-i\nu_1 t} \rho_{ca} + \text{c.c.}],$$
$$\dot{\rho}_{a'a'} = -\Gamma_{a'}\rho_{a'a'} + \Gamma_{aa'}\rho_{aa},$$
$$\dot{\rho}_{b'b'} = -\Gamma_{b'b}\rho_{b'b'} + \Gamma_{ab'}\rho_{aa} + \Gamma_{a'b'}\rho_{a'a'} + \Gamma_{bb'}\rho_{bb},$$
$$\dot{\rho}_{c'c'} = -\Gamma_{c'c}\rho_{c'c'} + \Gamma_{ac'}\rho_{aa} + \Gamma_{a'c'}\rho_{a'a'} + \Gamma_{cc'}\rho_{cc}.$$

Note that the density-matrix elements $\rho_{\alpha\beta}$ represent the population (coherence) for $\alpha = \beta$ ($\alpha \neq \beta$), and $\rho_{\alpha\beta}^* = \rho_{\beta\alpha}$. The population decay rates associated with the excited electronic states Γ_a and $\Gamma_{a'}$ are the sum of the contributions from spontaneous decay, RET, and collisional quenching rates. The decay rate $\Gamma_{\alpha\alpha'}$ ($=10\Gamma_{\alpha'\alpha}$) is considered to be equal to the RET rate. The decay rate corresponding to the electronic transitions is $\gamma_{aj} = (\Gamma_a + \Gamma_{jj'})/2 + \gamma_{aj}^{pd}$ ($j \rightarrow b, c$) and that corresponding to the Raman transition γ_{bc} is primarily the RET rate. Here γ_{aj}^{pd} represents pure coherence depashing in the $|a\rangle \leftrightarrow |j\rangle$ transition. For details of the decay model considered here, see Ref. [7].

To separate the molecular polarizations oscillating at different frequencies and to remove the fast oscillating terms in the density-matrix equations, we used the following canonical transformations:

$$\rho_{ac}(t) = \sigma_{ac}(t)e^{-i\nu_1 t} + \eta_{ac}(t)e^{-i\nu_4 t},$$
$$\rho_{ab}(t) = \sigma_{ab}(t)e^{-i\nu_2 t} + \eta_{ab}(t)e^{-i\nu_3 t}, \qquad (7)$$
$$\rho_{bc}(t) = \tilde{\rho}_{bc}(t)e^{-i(\nu_1 - \nu_2)t},$$

where ν_4 is the frequency of the generated ERE-CARS signal. To obtain the equations in the transformed frame, we dropped the fast terms oscillating at $e^{\pm i\delta t}$ with the assumption that $\delta \gg t^{-1}$. Note that 16 coupled differential equations are obtained after substituting Eqs. (7) into Eqs. (6), which describe the dynamical evolution of the molecular states and coherences.

III. ULTRAFAST EVOLUTION IN THE ERE-CARS CONFIGURATION

To obtain an analytical understanding of the evolution of ERE-CARS polarization, let us evaluate the coherence η_{ac} that oscillates at ν_4, representing the instantaneous CARS polarization. The equation of dynamics for the matrix element η_{ac} after applying the transformations (7) to Eqs. (6) is

$$\frac{\partial \eta_{ac}(t)}{\partial t} = -(\gamma_{ac} + i\Delta)\eta_{ac}(t) + i\Omega_3(t)\tilde{\rho}_{bc}(t). \qquad (8)$$

Here $\gamma_{ac} = \frac{1}{2}(\gamma_a + \gamma_c) + \Gamma_{ac}^{PD}$ is the total coherence decay associated with the $|a\rangle \leftrightarrow |c\rangle$ transition. Expanding Eq. (8) in a Taylor series for $\Omega_3 \rightarrow 0$, a formal solution of the coherence to the first order in Ω_3 can be obtained using an integrating factor [33]

$$\alpha(t) = \exp\left[\int_0^t (\gamma_{ac} + i\Delta)dt'\right], \qquad (9)$$

which leads to the formal solution for coherence η_{ac} to the first order in the probe [34]

$$\eta_{ac}^{(1)}(t) = ie^{-(\gamma_{ac} + i\Delta)t} \int_{t_{30} - \tau_3}^t \Omega_3(t')\tilde{\rho}_{bc}^{(0)}(t')e^{(\gamma_{ac} + i\Delta)t'}dt'. \qquad (10)$$

If the probe delay is much longer than the durations of the pump and Stokes pulses, we assume that the probe delay $t_3 - t_1$ is much longer than t_1 and t_2; then we can assume that the zeroth-order Raman coherence (in the absence of the probe) remains constant within the duration of the probe, i.e.,

$$\tilde{\rho}_{bc}^{(0)}(t) \equiv \bar{\rho}_{bc} \qquad (11)$$

is a constant within the limit $t_3 - \tau_3 < t \ll \gamma_{bc}^{-1}$. For the Gaussian probe appearing within this time window, the coherence in the ERE-CARS transition can be obtained (with $\Delta = 0$) as

$$\eta_{ac}^{(1)}(t) = (i/2)\sqrt{\pi}e^{\gamma_{ac}t_3 + (\gamma_{ac}\tau_3/2)^2}\bar{\rho}_{bc}\Omega_{30}\tau_3 e^{-\gamma_{ac}t}$$
$$\times \left[\text{erf}\left(1 + \frac{\gamma_{ac}\tau_3}{2}\right) + \text{erf}\left(\frac{t - t_{30}}{\tau_3} - \frac{\gamma_{ac}\tau_3}{2}\right)\right]. \qquad (12)$$

Note that the above coherence is purely imaginary because we have considered $\Delta = 0$. At a longer time limit $t \rightarrow \gamma_{bc}^{-1}$, the error functions remain unchanged but the coherence $\eta_{ac}(t)$ decays to become zero at a time $t \gg \gamma_{ac}^{-1}$. However, for an intense probe, the above result will become invalid because

the intense probe can perturb the ground-state coherence ρ_{bc}, as will be discussed later with reference to Fig. 2(c) obtained from the numerical solutions.

Under the same condition as above and assuming the limiting case of $\gamma_{ac} \to 0$ and $(t_3 - \tau_3) \to -\infty$, the integral in Eq. (8) reduces to the transient pulse area of the probe pulse $\theta_3(t)$; thus

$$\eta_{ac}^{(1)} = \left(\frac{i}{2}\right)\bar{\rho}_{bc}\theta_3(t), \qquad (13)$$

where θ_3 is defined as [22]

$$\theta_3(t) = \int_{-\infty}^{t} 2\Omega_3(t')dt'. \qquad (14)$$

From Eq. (13) it is clear that the instantaneous ERE-CARS polarization is proportional to the pulse area of the probe field under the weak-probe condition. For the Gaussian probe pulse under consideration, the transient polarization $\eta_{ac}^{(1)}$ can be rewritten as

$$\eta_{ac}^{(1)} = i\sqrt{\pi}\,\bar{\rho}_{bc}\Omega_{30}\tau_3. \qquad (15)$$

Here Ω_{30} is the peak Rabi frequency over the duration of the probe pulse. Thus, the coherence $\eta_{ac}^{(1)}$ is proportional to τ_3. Even though the above result is obtained in a weak-probe condition, the result depicts the underlying physics for the existence of a threshold criterion for saturation of the ERE-CARS signal. Since the value of any coherence can reach a maximum value of only 0.5, the threshold Rabi frequency of the probe for

saturation of $\eta_{ac}^{(1)}$ is inversely proportional to the duration of the pulse. However, note that the assumption (11) that is used to obtain the above solution clearly indicates that the pulse-area-based solution may not be valid for probe durations $\tau_3 > \gamma_{bc}^{-1}$. Later in the paper, we show from our numerical calculations that the above saturation condition is indeed not valid if the pulses are longer than the effective decay time scale. It has been shown earlier that with ultrafast-laser excitations, the absorption and fluorescence in a two-level system saturate when the area under the driving pulse reaches $\pi/2$ and π, respectively [22].

In a real ERE-CARS experiment, the probe must be much stronger if an acceptable SNR is to be achieved. Hence, to obtain a solution for ERE-CARS polarization under strong probe conditions, we obtain a numerical solution to study the ERE-CARS dynamics. We consider the dynamics of the molecular-state population (ρ_{aa} and ρ_{bb}) and Raman coherence (ρ_{bc}) for ultrafast pump, Stokes, and probe pulses and also determine how the instantaneous ERE-CARS polarization η_{ac} (and hence the ERE-CARS signal) evolves with the ultrafast pulses. The coupled density-matrix equations are solved numerically using a fifth-order Runge-Kutta method and the results are presented in Fig. 2. While keeping the values of the peak intensities of the pump and Stokes pulses unchanged at $I_{10} = I_{20} = 10^{10}$ W/m^2, we vary the peak intensity of the probe field I_{30} parametrically, ranging between 10^{11} and 10^{18} W/m^2. For all of the numerical results, we consider the pump-, Stokes-, and probe-pulse durations to
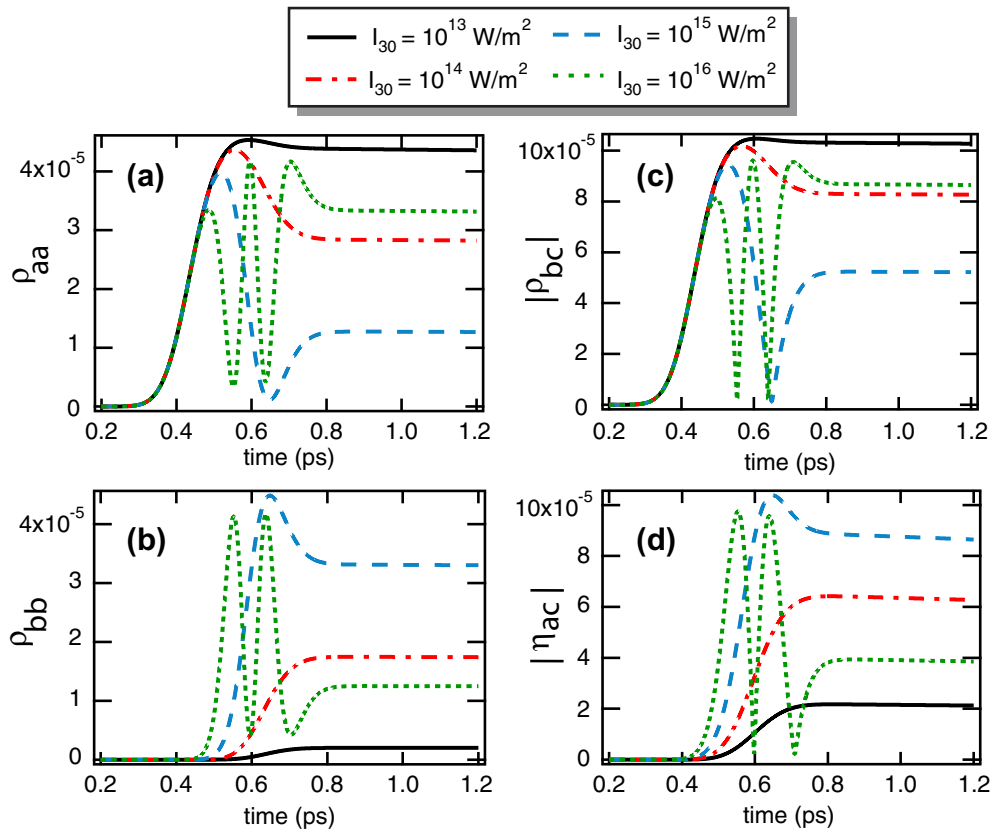

FIG. 2. (a) Population in the excited electronic state $|a\rangle$, (b) excited vibrational state $|b\rangle$, (c) ground-state (Raman) coherence, and (d) instantaneous polarization in the ERE-CARS transition for different probe intensities. The following parameters are used for the plot: the peak of the pump and Stokes pulse appears at 400 fs and the probe delay is maintained at 200 fs.

be $\tau_i = 100$ fs. The peak of the pump and Stokes pulses appears at $t_1 = t_2 = 400$ fs. As in a typical femtosecond CARS experiment, we consider the probe delay to be 200 fs and hence $t_3 = 600$ fs. Note that assuming the beam diameter to be 100 μm, the peak intensity of the probe $I_{30} = 10^{11}$ W/m^2 corresponds to laser energies of 1.4 nJ, 140 pJ, and 14 pJ at probe durations $\tau_3 = 1$ ps, 100 fs, and 10 fs, respectively. The maximum value of $I_{30} = 10^{18}$ W/m^2 corresponds to laser energies of 14 mJ, 1.4 mJ, and 140 μJ for $\tau_3 = 1$ ps, 100 fs, and 10 fs, respectively. Such laser energies are readily available in commercial high-power lasers. For example, a Ti:sapphire laser operating at 800 nm at 6 mJ per pulse laser energy generating 100-fs pulses can produce about 20 μJ at 236 nm using a tunable optical parametric amplifier.

Figure 2(a) shows that for the weaker probe $I_{30} < 10^{14}$ W/m^2, the population in the excited electronic state ρ_{aa} reaches a maximum at ~600 fs, i.e., when the peak of the probe pulse appears. However, since the duration of the pulse is very short compared to the molecular response time, the excited-state population does not follow the probe pulse during the tail end of the pulse; later, ρ_{aa} decays with a characteristic decay rate Γ_a of the state $|a\rangle$. For higher probe intensities, the transition saturates even before the peak of the probe pulse appears at t_3; hence, the maximum achievable value of ρ_{aa} is reduced. For $I_{30} \geqslant 10^{14}$ W/m^2, the Rabi oscillation is observed in ρ_{aa} after the onset of saturation. Once the probe pulse leaves the molecule, the population decays at the rate Γ_a. Similarly, the population ρ_{bb} in the excited rovibrational state $|b\rangle$ (in the ground electronic state) in Fig. 2(b) exhibits a monotonic increase initially when the pump and Stokes pulses are present. It reaches a quasi-steady-state for the time interval $t_3 < t \ll \gamma_{bc}^{-1}$ in the absence of the probe (not shown here). However, since the resonant coupling of the probe pulse with $|a\rangle \leftrightarrow |c\rangle$ transition is orders of magnitude stronger than the Raman coupling by pump and Stokes pulses with $|b\rangle \leftrightarrow |c\rangle$, once the probe pulse is turned on, the probe takes away molecular population from state $|b\rangle$ to populate state $|a\rangle$. Thus, ρ_{bb} remains low compared to ρ_{aa}, even for weaker probe intensities. However, once the probe transition is saturated and after the onset of Rabi oscillation, the population oscillates between $|a\rangle$ and $|b\rangle$, but their values remain out of phase by π. Note that for the delayed resonant probe considered here, the population in the probe transition oscillates as it does in a resonant two-level system [22].

The ground-state coherence $|\rho_{bc}|$ is also plotted in Fig. 2(c), which shows behavior similar to that of ρ_{bb}; however, they are out of phase by π. For stronger probe pulses, ρ_{bc} shows Raman-saturation-like oscillations, which were described by the two-photon pulse area approach [21,22]. However, note that the origin of the ultrafast oscillations in those references was because of saturation of the Raman transition by strong pump and Stokes pulses, unlike in the current study where the amplitude of Raman coherence is well below its maximum value of 0.5. Here the resonant probe pulse causes oscillation of the population in the state $|b\rangle$, resulting in oscillation in ρ_{bc}. In Fig. 2(d) we present the coherence $|\eta_{ac}(t)|$ that depicts the generated instantaneous ERE-CARS polarization or the square root of the transient ERE-CARS signal. For a weak probe, the coherence η_{ac} shows an asymmetric structure in time, reaching the maximum when the peak of the probe pulse appears. In

the next section we consider saturation of the integrated ERE-CARS signal.

IV. ULTRAFAST SATURATION OF ERE-CARS

To investigate saturation of ERE-CARS with a strong probe, if we assume that the excitation of ρ_{aa} in the probe transition $|b\rangle \leftrightarrow |a\rangle$ is equivalent to an isolated two-level transition [22] and that the ERE-CARS signal is proportionally dependent on ρ_{aa}, we may predict that the ERE-CARS signal will saturate once the total pulse area reaches π, i.e.,

$$\Theta_3 = \lim_{t \to \infty} \theta_3(t) = 2\Omega_{30}\tau_3\sqrt{\pi} \geqslant \pi. \qquad (16)$$

This relation shows that the saturation threshold of the Rabi frequency is inversely proportional to the pulse duration and hence the threshold intensity of the probe for saturation of ERE-CARS signal is quadratically dependent on the inverse of the pulse duration, i.e.,

$$I_{30}^{\text{th}} = \frac{2^3 |\vec{d}_{ac}|^2}{\hbar^2 \pi c \epsilon_0} \tau_3^{-2}, \qquad (17)$$

where c and ϵ_0 are the speed of light and the permittivity in vacuum, respectively. Note that since the ERE-CARS configuration is more complex and the signal is dependent on the Raman coherence, we numerically investigate the saturation of the ERE-CARS signal for ultrafast excitation.
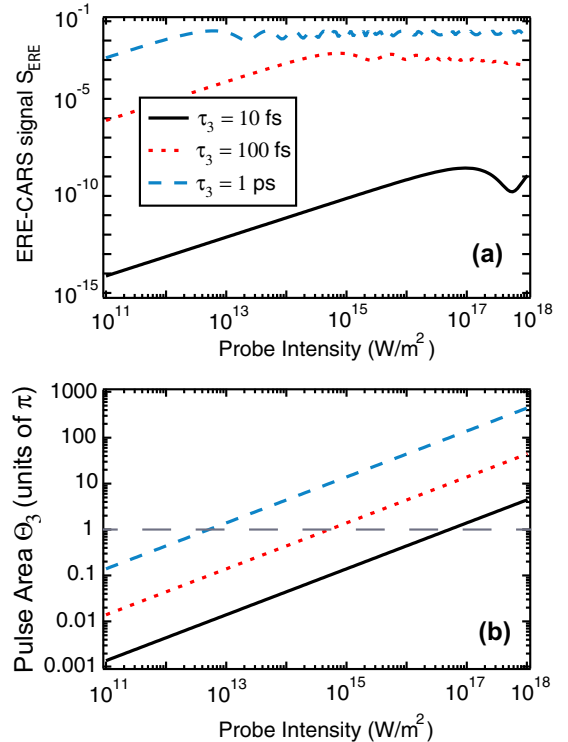

FIG. 3. Saturation of ERE-CARS signal intensity for different pulse durations in the hybrid ERE-CARS configuration. Pump- and Stokes-pulse durations are maintained at $\tau_1 = \tau_2 = 100$ fs and only the probe-pulse duration τ_3 is varied. (a) The ERE-CARS signal S_{ERE} plotted as a function of peak intensity of the probe I_{30} and (b) pulse area Θ_3 corresponding to I_{30}.

In Fig. 3 we present the numerical results to verify the above prediction. We consider three different probe-pulse durations ($\tau_3 = 1$ ps, 100 fs, and 10 fs) while maintaining the durations of the pump and Stokes pulses at $\tau_1 = \tau_2 = 100$ fs. Typically, the CARS configurations with probe durations different from those of the pump and Stokes pulses are called hybrid-CARS configurations [35–37] and the current configuration may be called a hybrid-ERE-CARS configuration. All parameters are assumed to have the same value as that in Fig. 2. In Fig. 3(a) we present the numerical solution of the integral of the square of the coherence $|\eta_{ac}|^2$ that represents integrated ERE-CARS signal

$$S_{\mathrm{ERE}} \propto \int_0^\infty |\eta_{ac}(t)|^2 dt \tag{18}$$

as a function of the probe intensity I_{30}. Clearly, the threshold intensity of the probe for saturation of the ERE-CARS signal increases by two orders of magnitude when the pulse duration of the probe decreases by one order of magnitude. This dependence is precisely captured in Eq. (15), even though Eq. (15) was obtained in the weak-probe-field limit.

Furthermore, Fig. 3(b) is a numerical plot of the pulse area corresponding to the probe intensities used on the x axis of Fig. 3(a). Comparing the Figs. 3(a) and 3(b), the ERE-CARS saturation threshold is reached once the pulse area corresponding to the probe area is larger than π. Note that Figs. 3(a) and 3(b) are plotted on a log-log scale. The saturation criterion agrees well with the 10- and 100-fs probe pulses. However, the Θ_3-based criterion slightly underpredicts the threshold limit of the Raman saturation for the picosecond probe by a small fraction of the actual Raman threshold. The reason for this is that the front end of the picosecond probe significantly overlaps with the pump and Stokes pulses, leading to population recycling between states $|b\rangle$ and $|c\rangle$ during the pulse excitation. Hence, the Θ_3-based criterion (17) is not exact for longer pulses, which was also mentioned in the discussion following Eq. (15). However, it lends a predictive capability to determine the saturation threshold of ultrafast ERE-CARS within an order of magnitude not only for the femtosecond probe but also for a range of pulse durations.

Note that the pulse-area-based saturation criterion is derived under the condition that the probe pulse is delayed with respect to the pump and Stokes pulses. To understand how the saturation criterion obtained from Θ_3 may be affected by the probe delay, we plotted the ERE-CARS signal in Fig. 4 as a function of I_{30} for different probe delays. We consider the duration of the probe pulse to be $\tau_3 = 100$ fs and all other parameters are maintained at the same values as in Fig. 3. The plots in Fig. 4 show that if the probe-pulse delay is zero or small ($t_{\mathrm{delay}} \leqslant \tau_3$), the saturation of the ERE-CARS signal occurs at a much larger value of I_{30} than that for $\tau_d \sim 200$ or 300 fs. For 100-fs pulse duration, $\Theta_3 = \pi$ for $I_{30} \approx 5 \times 10^{14}$ W/m². Thus, the Θ_3-based criterion underpredicts the saturation threshold for small or no probe delays. This discrepancy may be caused by significant repopulation of state $|b\rangle$ in the presence of the pump and Stokes pulses. For a probe delay of ~200 fs, the saturation-threshold intensity follows the pulse-area-based criterion of $\Theta_3 \geqslant \pi$. Once again, the Θ_3-based criterion underpredicts the threshold intensity for probe delays in excess of 400 fs. The saturation threshold

continues to increase for even larger probe delays. Such a discrepancy could be caused by a decrease in the population in $|b\rangle$ and hence the Raman coherence ρ_{bc} because of population transfers to $|b'\rangle$ via RET during the long-delayed period, reducing the total ERE-CARS polarization. Hence, the threshold intensity for saturation of ERE-CARS increases. For pump- and Stokes-pulse intensities well below the Raman saturation condition, the θ_3-based criterion is accurate if we can temporally isolate the determining transition of interest but within the limit that the probe delay is much smaller than the effective decay rate of the system. However, in all of the above cases, the Θ_3-based criterion predicts the saturation threshold for probe intensity accurately within one order of magnitude.

V. COMPARISON OF ERE-CARS SATURATION IN LONG- AND SHORT-PULSE DURATION REGIMES

In the previous section we demonstrated in Fig. 3 that the threshold intensity of saturation of S_{ERE} is a function of the duration of the probe pulse [as also shown in Eq. (17)]. However, from the earlier literature on ERE-CARS, we know that if the peak intensity of the probe transition is increased such that the Rabi frequency of the probe is larger than the effective decay rate of the transition, the onset of a Rabi oscillation between the states $|a\rangle \leftrightarrow |b\rangle$ engages the population of those states through the interaction with the probe pulse. If we increase the number of photons further (or increase the peak intensity), the new photons do not have an opportunity to interact with the molecule and hence can no longer be absorbed, leading to the absorption saturation in the $|a\rangle \leftrightarrow |b\rangle$ transition; in general, this is also referred to as the transition being saturated. For cw or long-pulse excitations, this condition can be achieved if the driven system reaches an underdamping regime; i.e., the peak Rabi frequency of the probe pulse is larger than the effective decay rate of the system, i.e.,

$$\Omega_{30} > \sqrt{\Gamma_{ac} \gamma_{ac}^{pd}}, \tag{19}$$

where $\Gamma_{ac} = \Gamma_a + \Gamma_{cc'}$ is the total population decay in the probe transition. It is clear from the above saturation condition that in the long-pulse-excitation regime the threshold intensity of the saturation is independent of the duration of the probe pulse τ_3, unlike in the ultrafast ERE-CARS results in Fig. 3. For absorption and fluorescence with short-pulse
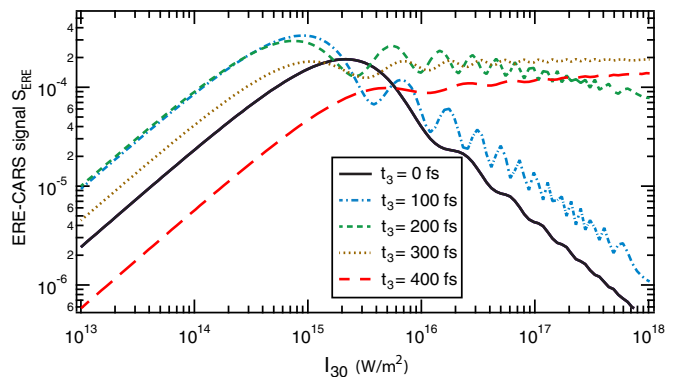

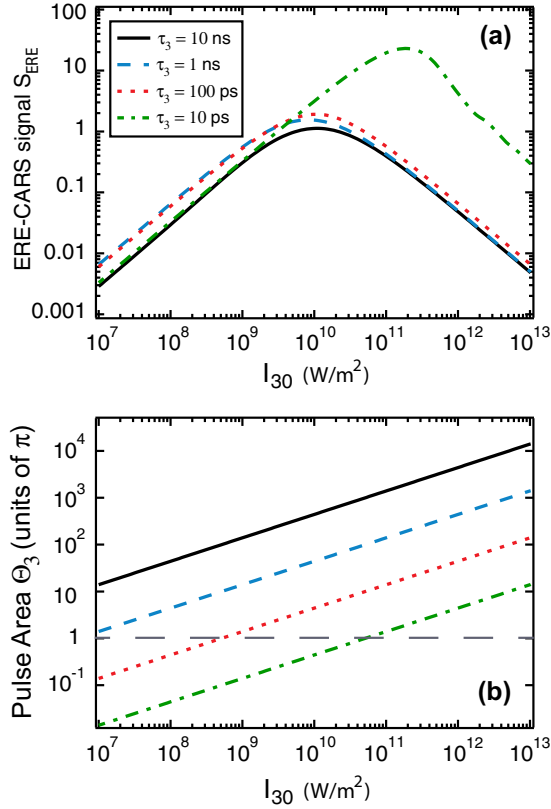FIG. 4. Saturation of ERE-CARS signal intensity for different probe delays.

FIG. 5. (a) Saturation of integrated ERE-CARS signal intensity for different pulse durations in the longer-pulse regime between 10 ns and 10 ps. (b) Pulse area corresponding to peak intensities of the probe pulse.
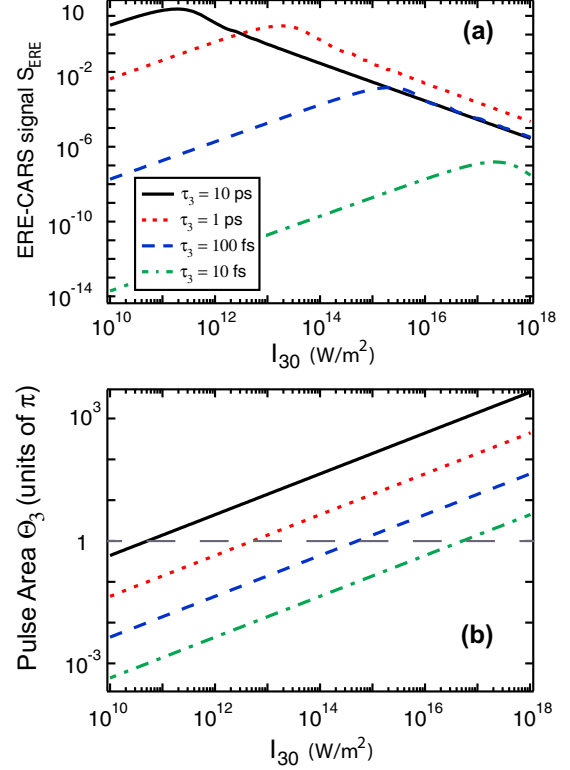

FIG. 6. (a) Saturation of integrated ERE-CARS signal intensity for different pulse durations in the shorter-pulse regime between 10 ps and 10 fs. (b) Pulse area corresponding to peak intensities of the probe pulse.

excitation, we have shown that the underdamping condition is *only* a necessary condition [22]. The ultrafast saturation of absorption and fluorescence occurs at a much higher intensity when the system reaches a transient-gain regime within the duration of the driving pulse. Therefore, for ERE-CARS it is important to compare the saturation of the signal for different probe-duration regimes to investigate what the ranges of pulse duration are where the saturation criterion transitions from a purely underdamping condition for long pulses to the transient-gain condition (Θ_3-based criteria) for the ultrafast saturation of the ERE-CARS signal.

In the following we compare the saturation of the ERE-CARS signal over an extensively wide range of durations of the probe pulse from 10 ns to 10 fs. For the purpose of clarity, we have plotted S_{ERE} for $\tau_3 \rightarrow$ 10 ns to 10 ps in Fig. 5(a) and $\tau_3 \rightarrow$ 10 ps to 10 fs in Fig. 6(a). To understand the validity of the Θ_3-based criteria described in the earlier section, we have also plotted the pulse area Θ_3 in Figs. 5(b) and 6(b), corresponding to the probe intensities used in Figs. 5(a) and 6(a), respectively. Note that in Fig. 3 we maintained the durations of the pump and Stokes pulses at $\tau_1 = \tau_2 = 100$ fs and only the probe-pulse duration τ_3 was varied. However, in Figs. 5 and 6 the durations of all three pulses are considered to be the same $\tau_1 = \tau_2 = \tau_3$ and they are varied simultaneously. Furthermore, real ultrafast ERE-CARS experiments may need to be performed with a probe delay to avoid any nonresonant background in the observed signal;

however, to ensure uniformity in the interaction conditions over a range of variation of six orders of magnitude of the probe-pulse duration, we maintain a zero probe-pulse delay in both Figs. 5 and 6. Also, to eliminate any saturation or saturationlike effect in Raman coherence caused by pump or Stokes pulses (as in Ref. [21]), we maintain the peak intensities of the pump and Stokes pulses at $I_{10} = I_{20} = 10^{10}$ W/m^2, where we have verified that Raman saturation does not occur even in the nanosecond regime.

The integrated ERE-CARS signal S_{ERE} for long pulses is plotted in Fig. 5(a). The signal increases until $I_{30} \sim 10^{10}$ W/m^2, but then it saturates and begins to decrease for the pulse durations from 10 ns to 100 ps, which corresponds to the peak Rabi frequency that is larger than the effective decay rate, as described in Eq. (19) for an underdamping regime. Clearly, the threshold intensity for saturation is independent of the probe pulse until the probe-pulse duration reaches $\tau_3 \sim 10$ ps, unlike the dependence described in Eq. (17) from the Θ_3 criterion. The pulse area Θ_3 corresponding to the different pulse durations, plotted in Fig. 5(b), shows that Θ_3 corresponding to the pulse durations for 10 ns and 100 ps are $\sim 500\pi$ and $\sim 50\pi$, respectively. For $\tau_3 = 100$ and 10 ps, the pulse area is $\Theta_3 \sim 4.5\pi$ and 1.9π, respectively. Clearly, for long pulses with durations much longer than the molecular dephasing time scales (~ 20 ps), the pulse-area-based criterion completely fails. The saturation threshold is determined only by the underdamping condition (19). As noted in Refs. [7,15], a significant repumping can occur during the duration of the

excitation pulse that has been really helpful for the quenching independence of the ERE-CARS signal in NO. However, for a pulse duration on the order of the dephasing time scale of the molecule, the underdamping condition is not a sufficient condition for saturation of the ERE-CARS signal.

We have plotted the ERE-CARS signal S_{ERE} for ultrashort pulses with durations ranging from 10 ps to 10 fs in Fig. 6(a). After the initial rise S_{ERE} saturates in each of the cases of the pulse durations of the probe but at very different I_{30}, unlike those in Fig. 5. The signal saturation in the ultrafast excitation regime with the probe-pulse duration shorter than the dephasing time scale may be understood as follows: The shorter the duration of the pulse compared to the effective decay time scale of the molecule, the higher the laser intensity needed to cause a Rabi cycle to occur within τ_3, which is necessary for the saturation of the probe transition. This process is very similar to that for the ultrafast saturation of fluorescence described in Ref. [22] and saturation of picosecond polarization spectroscopy [25,26]. The ultrafast saturation of S_{ERE} follows the Θ_3-based criterion obtained in Eq. (17), i.e., the threshold intensity of saturation of S_{ERE} increases quadratically with a decrease in the duration of the probe pulse τ_3. The pulse area corresponding to each τ_3 is plotted in Fig. 6(b). In each case of τ_3, the saturation of S_{ERE} follows the predicted pattern of Eq. (17), but the criterion slightly underpredicts the saturation threshold by a factor of 2. The reason is that we have assumed the probe delay to be zero for all of the cases where in the presence of all three fields, some active repopulation may be occurring in states $|b\rangle$ and $|a\rangle$, pushing the threshold of saturation higher. This result follows the discussion of the role of probe delays presented in the previous section. As shown earlier, the Θ_3-based criterion will be exact for ultrafast saturation of ERE-CARS if the probe delay is maintained within two to three times the probe pulse duration. The predicted threshold of saturation agrees well with the all-resonant ERE-CARS experiments carried out recently [38].

It may be noted that since the resonant probe-pulse intensities needed for saturation are very high, it may cause an ac Stark shift or ionization of NO via two-photon transitions from $X\,^2\Pi(v=1)$. Little literature exists on the ultrafast UV-laser excitation of NO, e.g., López-Marten *et al.* have shown that the laser intensities in excess of 10^{17} W/m^2 with a 140-fs pulse operating at 410 nm can cause the ac Stark shift via a two-photon transition [39]; also, a laser peak intensity of 2×10^{17} W/m^2 at 265 nm (40–60 fs) has been used in conjunction with a probe at 400 nm to ionize NO via resonant excitation of an intermediate level to observe the ac Stark shift (see Ref. [40]). Though no study has been reported for ionization of NO by an UV pulse of 236 nm at 10 fs, from the reported experiments of NO with a 200-fs pump at 800 nm [41], we believe no significant ionization would occur before the saturation threshold of the ERE-CARS signal limit is reached, even for the 10-fs excitation.

VI. SUMMARY

We have obtained a simplified criterion for the saturation threshold for the intensity of the ultrafast resonant probe in an ERE-CARS configuration. Our criterion holds rather well for a range of ultrashort pulse durations that are effectively delayed with respect to the pump and Stokes pulses. We have compared the threshold of saturation of the probe between pulse durations ranging from 10 ns to 10 fs and have shown how the physical mechanism of saturation differs between the long- and short-pulse regimes and hence the saturation criterion differs. The underdamping condition is a sufficient condition for saturation of ERE-CARS in the long-pulse regime, leading threshold intensity to be the same for up to 100-ps durations. However, for ultrafast ERE-CARS, an additional condition must be satisfied that the probe transition must change from transient absorption to the transient-gain regime; hence, with a pulse-area-based calculation, we obtained a criterion that predicts the ERE-CARS saturation threshold intensity of the probe pulse for durations ranging from 10 ps to 10 fs within one order of magnitude. In the ultrashort-pulse-excitation regime, the saturation-threshold intensity is quadratically dependent on the inverse of the pulse duration, unlike in the long-pulse regime. The pulse-area-based study may be generalized to obtain thresholds for saturation of multiphoton processes [42], laser-induced breakdown [43], ionization or other nonlinear optical processes in a variety of systems that employ the ultrafast excitation, and different pulse shapes [44,45].

ACKNOWLEDGMENTS

---

[1] S. Roy, J. R. Gord, and A. K. Patnaik, Prog. Energy Combust. Sci. **36**, 280 (2010).

[2] S. F. Hanna, W. D. Kulatilaka, Z. Arp, T. Opatrny, M. O. Scully, J. P. Kuehner, and R. P. Lucht, Appl. Phys. Lett. **83**, 1887 (2003).

[3] S. A. J. Druet, B. Attal, T. K. Gustafson, and J. P. Taran, Phys. Rev. A **18**, 1529 (1978).

[4] B. Attal-Trétout, S. C. Schmidt, E. Crété, P. Dumas, and J. P. Taran, J. Quant. Spectrosc. Radiat. Transfer **43**, 351 (1990).

[5] M. Schenk, T. Seeger, and A. Leipertz, Appl. Opt. **44**, 4157 (2005).

[6] S. Roy, W. D. Kulatilaka, S. V. Naik, N. M. Laurendeau, R. P. Lucht, and J. R. Gord, Appl. Phys. Lett. **89**, 104105 (2006).

[7] A. K. Patnaik, S. Roy, J. R. Gord, R. P. Lucht, and T. B. Settersten, J. Chem. Phys. **130**, 214304 (2009).

[8] W. D. Kulatilaka, N. Chai, S. V. Naik, N. M. Laurendeau, R. P. Lucht, J. P. Kuehner, S. Roy, and J. R. Gord, Opt. Lett. **31**, 3357 (2006).

[9] N. Chai, W. D. Kulatilaka, S. V. Naik, N. M. Laurendeau, R. P. Lucht, J. P. Kuehner, S. Roy, V. R. Katta, and J. R. Gord, Appl. Phys. B **88**, 141 (2007).

[10] W. D. Kulatilaka, N. Chai, S. V. Naik, S. Roy, N. M. Laurendeau, R. P. Lucht, J. P. Kuehner, and J. R. Gord, Opt. Commun. **274**, 441 (2007).

[11] N. Chai, S. V. Naik, N. M. Laurendeau, R. P. Lucht, S. Roy, and J. R. Gord, Appl. Phys. Lett. **93**, 091115 (2008)

[12] J. P. Kuehner, S. V. Naik, W. D. Kulatilaka, N. Chai, N. M. Laurendeau, R. P. Lucht, M. O. Scully, S. Roy, A. K. Patnaik, and J. R. Gord, J. Chem. Phys. **128**, 174308 (2008).

[13] A. C. Eckbreth, *Laser Diagnostics for Combustion Temperature and Species* (Gordon and Breach, Amsterdam, 1996).

[14] N. Chai, R. P. Lucht, W. D. Kulatilaka, S. Roy, and J. R. Gord, J. Chem. Phys. **133**, 084310 (2010).

[15] A. K. Patnaik, S. Roy, R. P. Lucht, and J. R. Gord, J. Mod. Opt. **55**, 3263 (2008).

[16] L. A. Rahn, R. L. Farrow, M. L. Koszykowski, and P. L. Mattern, Phys. Rev. Lett. **45**, 620 (1980).

[17] R. Altkorn and R. Zare, Annu. Rev. Phys. Chem. **35**, 265 (1984).

[18] R. P. Lucht, R. L. Farrow, and D. J. Rakestraw, J. Opt. Soc. Am. B **10**, 1508 (1993).

[19] O. Kinrot and Y. Prior, Phys. Rev. A **50**, R1999 (1994).

[20] R. P. Lucht and R. L. Farrow, J. Opt. Soc. Am. B **5**, 1243 (1988).

[21] A. K. Patnaik, S. Roy, and J. R. Gord, Phys. Rev. A **87**, 043801 (2013).

[22] A. K. Patnaik, S. Roy, and J. R. Gord, Phys. Rev. A **90**, 063813 (2014).

[23] R. W. Boyd, *Nonlinear Optics* (Academic, San Diego, 1992).

[24] W. Demtroder, *Laser Spectroscopy, Vol. 2: Experimental Techniques* (Springer, Berlin, 2008).

[25] T. A. Reichardt, F. D. Teodoro, R. L. Farrow, S. Roy, and R. P. Lucht, J. Chem. Phys. **113**, 2263 (2000).

[26] S. Roy, R. P. Lucht, and T. A. Reichardt, J. Chem. Phys. **116**, 571 (2002).

[27] S. L. McCall and E. L. Hahn, Phys. Rev. Lett. **18**, 908 (1967).

[28] G. M. Genkin, Phys. Rev. A **58**, 758 (1998).

[29] R. Kienberger and F. Krausz, in *Few-Cycle Laser Pulse Generation and Its Applications*, edited by F. X. Kärtner (Springer, Berlin, 2010).

[30] L. Yuan, G. O. Ariunbold, R. K. Murawski, D. Pestov, X. Wang, A. K. Patnaik, V. A. Sautenkov, A. V. Sokolov, Y. V. Rostovtsev, and M. O. Scully, Phys. Rev. A **81**, 053405 (2010).

[31] G. Heck, A. Filin, D. A. Romanov, and R. J. Levis, Phys. Rev. A **87**, 023419 (2013).

[32] Y. Yonemaru, A. F. Palonpon, S. Kawano, N. I. Smith, S. Kawata, and K. Fujita, Phys. Rev. Appl. **4**, 014010 (2015).

[33] G. B. Arfken and H. J. Weber, *Mathematical Methods for Physicists*, 6th ed. (Academic, Amsterdam, 2005).

[34] M. Abramowitz and I. A. Stegun, *Handbook of Mathmatical Functions* (Dover, New York, 1972).

[35] B. D. Prince, A. Chakraborty, B. M. Prince, and H. U. Stauffer, J. Chem. Phys. **125**, 044502 (2006).

[36] D. Pestov, R. K. Murawski, G. O. Ariunbold, X. Wang, M. Zhi, A. V. Sokolov, V. A. Sautenkov, Y. V. Rostovtsev, A. Dogariu, Y. Huang, and M. O. Scully, Science **316**, 265 (2007).

[37] H. U. Stauffer, J. D. Miller, M. N. Slipchenko, T. R. Meyer, B. D. Prince, S. Roy, and J. R. Gord, J. Chem. Phys. **140**, 024316 (2014).

[38] S. Roy, H. U. Stauffer, J. Schmidt, P. Wrzesinski, and J. R. Gord (unpublished).

[39] R. B. López-Martens, T. W. Schmidt, and G. Roberts, Phys. Rev. A **62**, 013414 (2000).

[40] Z. Sun, H. Liu, N. Lou, and S. Cong, Chem. Phys. Lett. **369**, 374 (2003).

[41] A. Talebpour, S. Larochelle, and S. L. Chin, J. Phys. B **30**, 1927 (1997).

[42] H. U. Stauffer, W. D. Kulatilaka, J. R. Gord, and S. Roy, Opt. Lett. **36**, 1776 (2011).

[43] E. W. Van Stryland, M. J. Soileau, A. L. Smirl, and W. E. Williams, Phys. Rev. B **23**, 2144 (1981).

[44] P. R. Berman, L. Yan, K.-H. Chiam, and R. Sung, Phys. Rev. A **57**, 79 (1998).

[45] A. K. Patnaik, S. Roy, and J. R. Gord, Phys. Scr. **T165**, 014031 (2015).